ARTICLE

Size-Selective Diffusion in Nanoporous but Flexible Membranes for Glucose Sensors

Hiroki Uehara,[†,*] Masaki Kakiage,[†,§] Miho Sekiya,[†] Daisuke Sakuma,[†] Takeshi Yamonobe,[†] Nao Takano[‡,∥] Antoine Barraud,[‡] Eric Meurville[‡,*] and Peter Ryser[‡]

[†]Department of Chemistry and Chemical Biology, Gunma University, Kiryu, Gunma 376-8515, Japan, [‡]Laboratoire de Production Microtechnique, Ecole Polytechnique Fédérale de Lausanne (EPFL), CH-1015 Lausanne, Switzerland. [§]Research Fellow of the Japan Society for the Promotion of Science. Present address: Department of Chemistry and Materials Science, Tokyo Institute of Technology. [∥]Present address: Sensile Medical AG, CH-4614 Hägendorf, Switzerland.

ABSTRACT A series of nanoporous membranes prepared from polyethylene-*block*-polystyrene were applied for size-selective diffusion of glucose and albumin molecules. Millimeter-sized test cells for characterization of such molecular diffusions were designed assuming an implantable glucose sensor. The prepared nanoporous membrane exhibits excellent flexibility and toughness compared to conventional nanoporous membranes of brittle alumina. Pore size of the membranes could be controlled from 5 to 30 nm by varying preparation conditions. All of these nanoporous membranes prepared in this study let glucose pass through, indicating a continuous pore connection through the entire thickness of the membrane in a few tens of micrometers. In contrast, membranes prepared under optimum conditions could perfectly block albumin permeation. This means that these vital molecules having different sizes can be selectively diffused through the nanoporous membranes. Such a successful combination of size selectivity of molecular diffusion in nanoscale and superior mechanical properties in macroscale is also beneficial for other devices requesting down-sized manufacture.

KEYWORDS: nanoporous · membrane · glucose · albumin · biosensor · block copolymer

Nanoporous membranes can be used as molecular or ionic separators for various applications, including medical devices. For separator applications, molecules or ions must be able to pass through the membrane pores across the entire membrane thickness. There are two approaches for preparing pass-through pores: arrangement of separated pores perpendicular to the membrane surface, and junctions of pore channels. The typical example for the former case is an alumina nanoporous membrane. The most remarkable characteristic of this membrane is the straightness of the pores even for thicknesses beyond the micrometer scale. Since the pore size is easily controlled by the anodizing voltage as well as the electrolyte employed for the anodization process, the nanoporous alumina membranes have been favorably utilized for biofiltration applications.[1,2] Molecular transport could also be controlled by changing the pore size of the membrane. Likewise, the through hole channels of silica having a few tens of nanometers radii can selectively carry smaller molecules but block the larger ones. Desai *et al.*[3,4] investigated the difference of molecular transport between glucose and some proteins, such as albumin and immunoglobulin G, through engineered silica membranes. Teramae *et al.*[5] also reported that silica nanochannels supported in micropores of an alumina membrane could perfectly shut out the albumin diffusion.

Since glucose is one of the most important molecules in living animals, glucose separation and transport control are necessary functions for some medical devices. It is well-known that the glucose concentration in blood fluctuates when the pancreatic function is impaired (Type 1 diabetes) or the response by the body to insulin diminishes (Type 2 and gestational diabetes). Both lead to abnormally high blood sugar levels (hyperglycemia), and monitoring glucose is thus a key for effective treatment of diabetes, becoming one of the most popular but serious diseases especially in advanced nations nowadays. An autonomous implantable biosensor equipped with such nanoporous membranes would enable long-term continuous monitoring of the glucose concentration, alleviating diabetic patients' physical pain caused by daily blood-drawing for screening. However, nanoporous alumina or silica membranes are very brittle, so it is difficult to manufacture an actual device, especially a millimeter-size implantable glucose sensor. In contrast, polymeric materials have superior flexibility and thus are expected to be alternative.

*Address correspondence to uehara@chem-bio.gunma-u.ac.jp, eric.meurville@epfl.ch.

Received for review December 19, 2008 and accepted March 13, 2009.

Published online March 26, 2009.
10.1021/nn8008728 CCC: $40.75

Recently, various approaches have been tried to prepare polymeric nanoporousmembranes. Block-copolymer (BCP) is a possible answer for preparing nanopores arranged perpendicularly to the membrane surface with the highest pore density.[6] BCP exhibits various types of microphase separation, depending on the component ratio of the different blocks. For a cylindrical structure, perpendicular arrangement is achievable for membranes thinner than the cylinder diameter due to the enhanced self-assembly of BCP molecules restricted in a limited space. Selective removal of targeted cylindrical blocks provides straight pores across the membrane thickness.[7−19] Russell *et al.*[20] prepared thin nanoporous membranes of polystyrene (PS) from PS-*block*-poly(methyl methacrylate) (PMMA) with homopolymer PMMA. One advantage of these straight pores of ultrathin films is the higher capacity of flux flow for separation. However, such a thin film itself is mechanically weak, so it must be supported on the other microporous membrane for actual manufacturing of the separator.[21] The orientation of the precursory cylindrical structure is effective for preparing straight pores but with thicker membranes. Hillmyer *et al.*[22−29] applied an extrusion technique with a channel die to various diblock and triblock copolymers and successfully obtained a series of nanoporous materials.

Over past one decade, we[30−41] have focused on the structural and property development of polyethylene (PE), which is the simplest molecular architecture but exhibits excellent properties, including toughness, flexibility, wear resistance, *etc*. Crystallization with chain orientation induced by various drawing techniques develops these resultant properties of PE materials, due to molecular disentanglement during drawing.[30−32,36,37,40,41] Concerning the structural development of PE, we[42] have also reported that nanoperiodic arrangement of crystal/amorphous phases could be obtained by tensile drawing and subsequent annealing of highly entangled PE. The entanglement trapping on the boundary between crystalline and amorphous phases was crucial for the preparation of such nanoperiodic assembling. These molecular entanglements may play a similar role of segmental linkages of BCP chains in terms of their stress transmission and location at the boundary between different phases. The obtained nanoperiodic structure of PE is applicable as a template material for the nanoporous membranes having the superior flexibility when the amorphous phases are selectively etched.

Therefore, we[43] tried a preparation of a nanoporous PE membrane from a BCP precursor. Crystallization procedure develops a bicontinuous crystalline−amorphous structure, similar to so-called double gyroid packing,[44] under the optimum conditions. The junction of the pore channels was successfully formed in such a nanoporous membrane by later removal of amorphous phases with acid etching. The excellent flexibility of this membrane also holds promise for various applications. It can be easily mounted or installed in the smallest space like a winding, which is beneficial for downsized medical devices, such as implantable glucose sensors[45,46] requesting nanoporous but flexible membrane for actual manufacturing and operation. These superior properties of the resultant nanoporous structure are ascribed to the interconnection of the residual PE backbones emphasizing a crystalline state. PE also has high chemical resistance, as evidenced by the chemical etching process mentioned above, which can be an advantage for biosensor application.

In this study, a series of nanoporous membranes with different pore sizes were prepared with controlling the etching conditions. Their mechanical properties were compared to those of a conventional alumina membrane. Also, the selective diffusion of glucose toward albumin with different molecular sizes was testified using a millimeter-sized cell designed assuming an implantable glucose sensor.

RESULTS AND DISCUSSION

The starting material was PE/PS diblock copolymer (PE-*b*-PS). A previous study[43] revealed that the bicontinuous crystalline and amorphous phases could be prepared by controlling crystallization conditions. The optimum crystallization was performed at 90 °C for 3 days after complete melting at 180 °C in a vacuum oven. The later etching with fuming nitric acid (FNA) selectively removes the amorphous phases, producing the nanoporous membranes. Figure 1a,b presents photographs of the nanoporous PE membrane prepared in this study. Etching time for membrane preparation was 30 min, where the most remarkable nanoporous morphology was achieved, as discussed below. The strip was cut into 10 mm × 30 mm from the overall etched membrane with a 15 μm thickness. It could be folded without breaking (Figure 1a). A slight diagonal line was seen after opening the fold (Figure 1b). In contrast, a nanoporous alumina membrane, which has been used for previous biomedical device application,[47] was easily broken into numerous small pieces when it was folded.

In order to test their applicability for downsized implantable glucose sensor applications, the millimeter-size cells were developed for characterization of glucose diffusion and albumin retention, as illustrated in Figure 1c. The tested membrane was set between two chambers (chambers A and B) and exhibited no solution leakage at the sealed interfaces. The solution of targeted molecules (glucose and bovine serum albumin (BSA) in this study) with a given concentration was loaded into chamber A, and diffused molecules into chamber B originally filled with pure water or 150 mM aqueous NaCl for the test with BSA were recorded *versus* holding time. The solutions in both chambers were continuously stirred during diffusion tests. The concentrations of glucose and BSA were monitored by refrac-

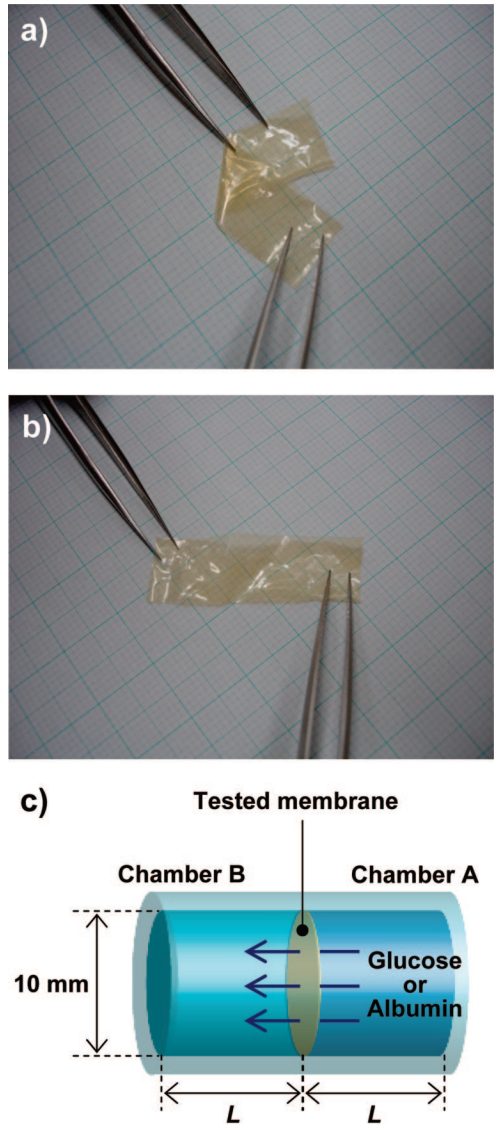

Figure 1. Photographs of nanoporous PE membrane prepared with an etching time of 30 min (a,b) and an illustration of diffusion/retention test cell designed assuming an implantable glucose sensor (c). This PE membrane was prepared with an etching time of 30 min and had a thickness of 15 μm. The strip was folded once diagonally in (a) and opened in (b), but it never broke due to the excellent flexibility of the nanoporous PE membrane. Such a testing membrane was sealed between chambers A and B in (c). Glucose or albumin solution with a given concentration was put in chamber A, and the concentration of permeating molecules in chamber B was monitored by refractometer scans or UV spectroscopy profiles during tests.

tometry and UV spectroscopy measurements, respectively (see Supporting Information, Figure S1).

Membrane Characterization. The mechanical characteristics of the nanoporous PE membrane prepared in this study were quantitatively evaluated by tensile tests. Figure 2 compares the stress−strain curves for the alumina membrane and the PE nanoporous membrane prepared with an FNA etching time of 30 min (same as Figure 1a,b). These tensile tests were made at room temperature. The alumina nanoporous membrane breaks at less than 3% elongation. In contrast, the

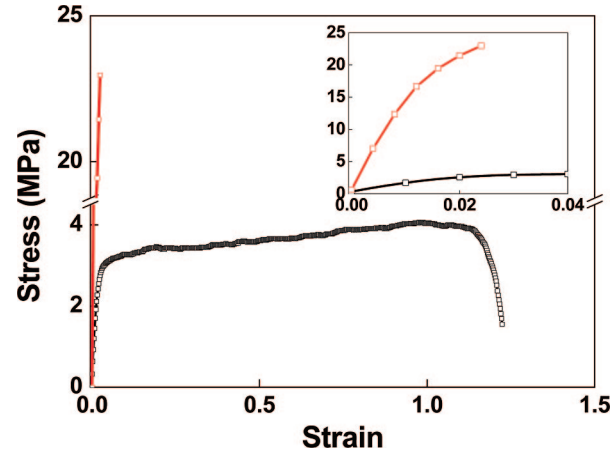

Figure 2. Comparison of stress−strain curves for the same nanoporous PE membrane prepared with an etching time of 30 min (black line) with commercial alumina membrane (red line). All tensile tests were made at room temperature. The nanoporous PE and alumina membrane have thicknesses of 15 and 60 μm. The inset enlarges the initial slope of the stress−strain curves until 4% strain.

nanoporous PE membrane exhibits excellent elongation exceeding 100% without breaking. The tensile modulus evaluated from the initial slope of the curve is much higher for the alumina membrane, as depicted in the inset of the figure, which enlarges the initial strain region. Together, these indicate that the alumina membrane is brittle, but the nanoporous PE membrane prepared in this study is tough.

It should be noted that the necking phenomenon was not observed for this nanoporous PE membrane. In contrast, an unetched precursory membrane exhibited apparent necking and much higher tensile stress (almost five times higher), indicating the destruction of the self-assembled bicontinuous crystalline−amorphous phase-separation system, which was also confirmed by electron micrograph observations.[48] Even for the precursory membrane, selective solvent swelling of the low-ductile PS components could eliminate such necking phenomena. Also, the tensile stress was reduced by half. As a result, the bicontinuity of crystalline PE and amorphous PS components could be retained even after tensile drawing up to 400% of strain when the above solvent swelling was applied. Similar reduction of the tensile stress and necking phenomena for the etched membrane in Figure 2 can be attributed to the removal of the low-ductile PS components. In contrast, Hillmyer *et al.*[49] obtained a nanoporous PS membrane from a cross-linked PS-*b*-poly(lactide) precursor. The elongation breaking point was limited to 10%, due to the low ductility of the remaining PS components.

The nanoporous morphologies of the prepared PE membranes were characterized by high-resolution field emission scanning electron microscopy (SEM). Figure 3 compares the surface images for the membranes prepared at different FNA etching times. These mem-

branes were 15 μm thick. The low-magnification images in the top column indicate that the network morphology of the surviving crystalline PE cylinders had spread across the whole area of the resultant membrane at least on a submillimeter scale (Figure 3a−d). Indeed, identical nanoporous morphologies were observed in several other portions of the membrane surfaces. This means that the nanoporous morphologies depicted in Figure 3 are characteristic of the corresponding membranes prepared at each FNA etching time.

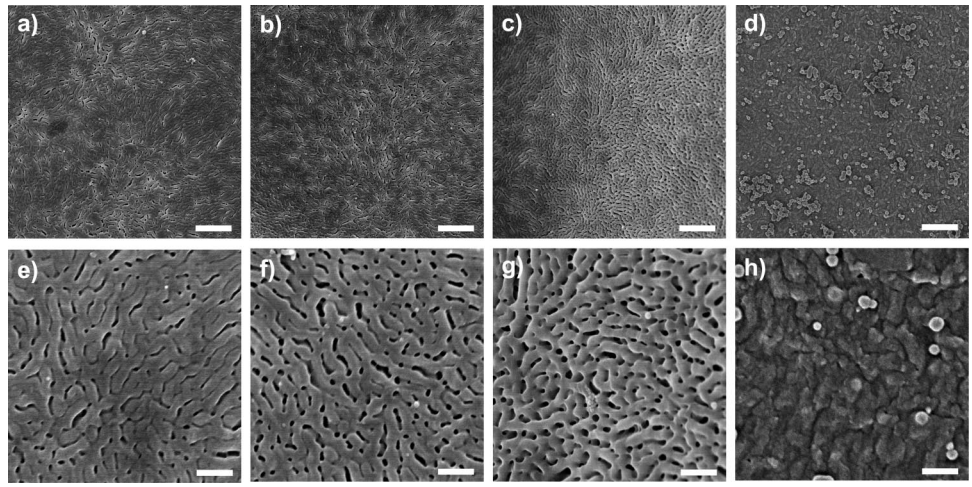

Figure 3. SEM images of the nanoporous membranes having different pore sizes. The etching was made at room temperature for 5 min (a,e), 10 min (b,f), 30 min (c,g), and 60 min (d,h). Top and bottom sets are low- and high-magnification images with scale bars of 1 μm (top) and 200 nm (bottom).

As depicted in the high-magnification images in the bottom column, narrow 5 nm wide pores are observed even for the shorter 5 min etching (Figure 3e). The 10 min etched membrane developed a pore width of 10 nm (Figure 3f). Such nanopores are attributed to amorphous PS components in microphase separation of the precursory PE-*b*-PS film.[43,48] In contrast, the crystalline PE components survived as an interconnected cylindrical structure after FNA etching. The network structure of the PE cylinders was clearly observed when the etching time was increased to 30 min (Figure 3g). Also, the PE cylinders gradually become thinner, due to the perfect removal of amorphous PS components surrounding the crystalline PE cylinders during 30 min etching, but then, the preferable fold resistance (Figure 1a,b) and toughness (Figure 2) were maintained by the residual PE backbone network. In other words, the junction of pore channels develops well. The estimated pore size was 30 nm. These results suggest that pore size is controllable by FNA etching time when preparing these nanoporous membranes. In contrast, the 60 min etched membrane surface has no pores (Figure 3h). The slight grooves imply the traces of pre-existing pores, but the PE cylindrical backbones were destroyed by prolonged etching, closing the pores. The spheres on the membrane are residual PS components removed from the membrane but aggregated on the membrane surface.

The membrane edge was also observed by fresh cleaving in liquid nitrogen. Figure 4 presents SEM images of the edge of the 10 min etched membrane. The network structure of the PE cylinders could be confirmed across the entire thickness of the membrane (15 μm). This means that narrow pore channels are interconnected within the entire membrane volume. Therefore, this nanoporous membrane is defined as a symmetrical structure, which is significantly different from the asymmetrical structure for the commercial nanoporous alumina membrane where an active thin layer is limited only on the surface with a 1 μm thickness.

Even for the other BCP precursors, selective removal of one component yields similar junction morphology of the pore channels. Recently, Lodge *et al.*[50] prepared nanoporous membranes from a bicontinuous microemulsion system containing BCP. Hillmyer *et al.*[49]

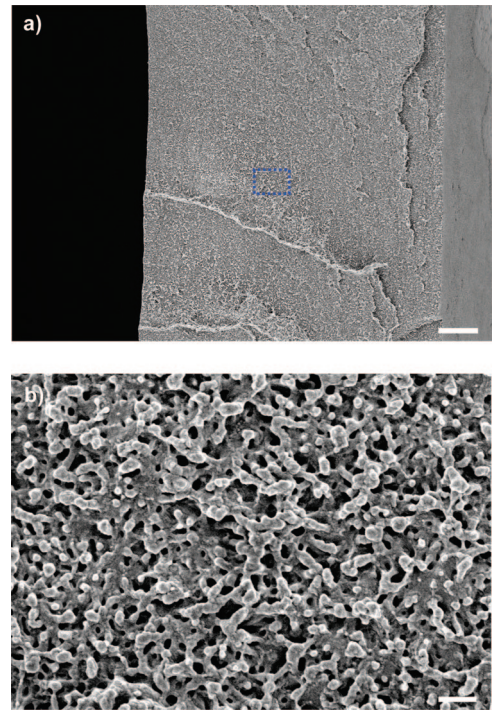

Figure 4. SEM images of the edge of the 10 min etched membrane with a 15 μm thickness. The prepared membrane was freshly cleft in liquid nitrogen before observation. (a) Entire image with a scale bar of 2 μm. The internal regions that are marked by the dotted blue line are enlarged in (b) with a scale bar of 200 nm.

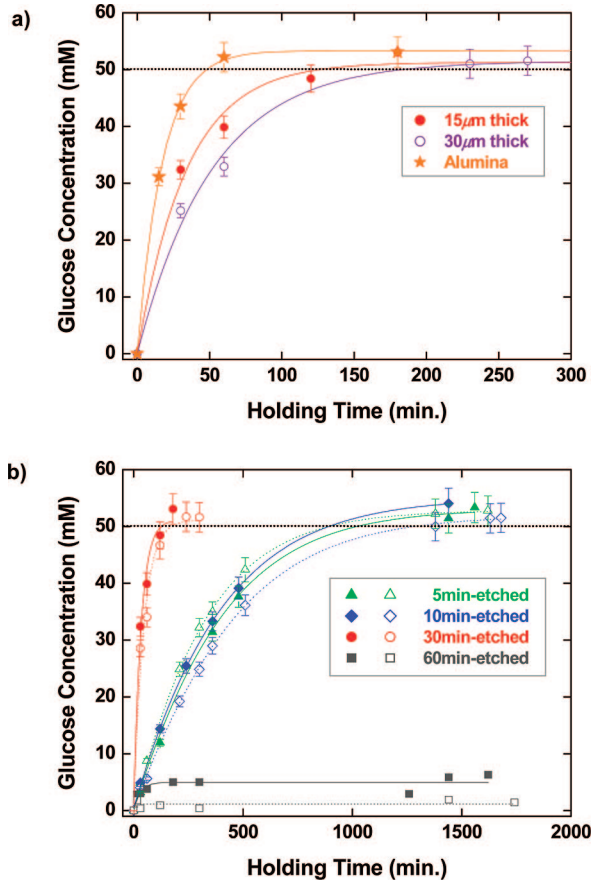

Figure 5. Glucose diffusion through nanoporous PE membranes prepared under different conditions. (a) Thickness effect and comparison with alumina membrane. Red filled circles (purple open circles) indicate the glucose concentration in the outlet chamber for two 30 min etched, 15 μm (30 μm) thick membranes as a function of holding time at room temperature. The data for the commercial alumina membrane are indicated by the filled orange star. The corresponding color lines are the results fitted by eq 1. (b) Effect of etching time for a series of 15 μm thick nanoporous PE membranes. The data of 5, 10, 30, and 60 min etched membranes are indicated by green triangles, blue diamonds, red circles, and gray squares, respectively. The filled legends and solid lines were obtained at the first run immediately after nanoporous membranes were set in a diffusion test cell. The open legends and dotted lines were obtained in the second run after the membranes were maintained in conical tubes with pure ethanol for 4 weeks. The theoretical maximum level of glucose diffusion is 50 mM (dotted thick line).

also utilized polymerization-induced phase separation to prepare bicontinuous precursor of BCP, resulting in nanoporous membranes. However, a control of a series of different pore sizes has not been reported.

Glucose Diffusion and Albumin Retention Behavior. First, the glucose diffusion characteristics of these nanoporous PE membranes were evaluated. Figure 5a plots the glucose concentration in the chamber B as a function of the holding time with solution stirring. It is well-known that molecular diffusion through various porous membranes is usually affected by the membrane thicknesses,[51] thus both 15 and 30 μm thick membranes were prepared at the same FNA etching time of 30 min. For comparison, the commercial alumina membrane was also tested under the same diffusion conditions. It was confirmed that a series of nanoporous morphologies for the 30 μm thick membranes prepared under corresponding etching times were similar to those for 15 μm thick ones (Figure S2 in Supporting Information). As seen in Figure 5a, both PE membranes can effectively diffuse the glucose molecules with time, but the thinner 15 μm thick membranes exhibit faster diffusion. Pore size estimated from SEM observation was 30 nm for both of these 30 min etched membranes (Figures 3g and Figure S2c in Supporting Information), which exceeds the glucose molecular size of 1 nm. However, the diffusion curve for the alumina membrane was steepest. These diffusion curves in Figure 5a are fitted by the exponential function

$$y = A\{1 - \exp(-x/\tau)\} \quad (1)$$

where y, x, A, and τ are glucose concentration, holding time, the equilibrium (maximum) concentration of glucose, and relaxation time of diffusion.[51] A is theoretically 50 mM because the initial 100 mM concentration of glucose should be equally divided in the two chambers having the same geometry and size. The obtained τ values were lowest for the alumina membrane (18 min), intermediate for the 15 μm thick PE membrane (34 min), and highest for the 30 μm thick membrane (52 min). The fast glucose diffusion for the alumina membrane is ascribed to its asymmetrical structure. The alumina membrane used here has a total thickness of 60 μm, but the active layer with 20 nm pores is only 1 μm thick at the outer surface. The other portions contain larger pores with 200 nm diameter. This means that the thinner membrane exhibits preferred diffusion of glucose when the pore size is of a similar scale.

Therefore, we compared the glucose diffusion characteristics of membranes with the same 15 μm thickness but different pore sizes. Figure 5b depicts the etching time effect for a series of 15 μm thick nanoporous PE membranes. The diffusion tests were performed both immediately after nanoporous membranes were set in the diffusion test cell (first run) and after the membranes were maintained in conical tubes with pure ethanol for 4 weeks (second run). Similar results were obtained for both membranes, meaning the nanoporous PE membranes were sufficiently durable. Here, two sets of the first runs were performed for the 60 min etched membrane because effective glucose diffusion was not observed in this case due to the pore collapse confirmed by SEM observation in Figure 3h. The glucose diffusion speed through membranes appears to correspond to the estimated pore size. The τ values calculated from the first runs of these membranes were 405 min for the 5 min etched membrane, 349 min for the 10 min etched membrane, and 34 min for the 30 min etched membrane. The remarkable difference in τ between 10 and 30 min etched membranes indicates the imperfect interconnection of pore channels for the shorter etching times.

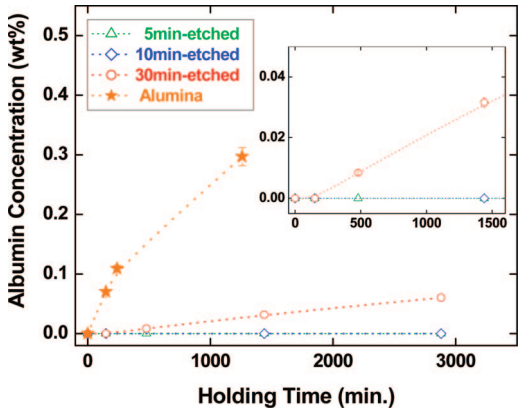

Figure 6. BSA retention for 15 μm thick nanoporous PE membranes prepared at different etching times. The meaning of the lines and legends are the same as in Figure 5b. The data for the commercial alumina membrane are also included. The theoretical maximum concentration of BSA is 0.5 wt %. The inset is an expanded view of the initial change with the shorter holding time up to 24 h for 5, 10, and 30 min etched membranes.

BSA retention was also characterized for this 15 μm thick series of nanoporous PE membranes. Three membranes exhibiting effective glucose diffusion in Figure 5b were selected; they were the 5, 10, and 30 min etched membranes. Figure 6 plots the BSA concentration in the chamber B as a function of the holding time with solution stirring. For comparison, the commercial alumina membrane was also tested under the same conditions. These experiments were performed after the glucose diffusion tests. The theoretical maximum concentration of BSA is 0.5 wt % because half of the initial 1.0 wt % concentration of BSA should be diffused into the chamber B in the equilibrium state. BSA diffusion takes longer than glucose diffusion due to the larger molecular size (7.1 nm in diameter).[5,52] All of the nanoporous PE membranes examined here retained BSA in the initial stage of holding time (at least 150 min). Among these membranes, both the 5 and 10 min etched membranes exhibited full retention of BSA even through 48 h holding. Such a similarity of the BSA diffusion data for these membranes coincides well with that of the glucose diffusion data in Figure 5b. Although molecular diffusion or separation properties of the polymeric nanoporous membranes were recently investigated,[20,52−54] full retention of BSA diffusion has not been reported.

In contrast, the 30 min etched membrane gradually leaks BSA up to 12% of the equilibrium concentration at a maximum holding time of 48 h, but this is still lower than those of the nanoporous alumina membranes, where the BSA leakage exceeds 50% at 24 h. It should be noted that the 30 min etched membrane fully retained BSA until 150 min, at which time glucose diffusion achieved the equilibrium state (see Figure 5). This means that the 30 min etched membrane is preferred for rapidly separating glucose and BSA for shorter holding times. The 30 min etched membrane can thus be used as separating application alone, depending on the targeted holding time. The longer glucose diffusion for the shorter etching times can be also improved by reducing the membrane thickness for implantable glucose sensor application which requires fast response time to glucose changes (*i.e.*, fast glucose diffusion) in interstitial fluid.

Diffusion/Retention Model for Nanoporous Membranes. The diffusion/retention characteristics of the nanoporous PE and alumina membranes are summarized in Figure 7. For the latter membrane, we focused on an asymmetrical surface-layer structure because it is actually more effective for size-selective separating of glucose and BSA molecules. When the solution contains both glucose (smaller red dots) and BSA (larger green particles), the glucose can fully diffuse through both membranes. In contrast, the PE membrane fully retains BSA, depending on the pore size and holding time. However, alumina membranes apparently leak the BSA even in the initial few minutes. These simulations are also supported by pore-size estimation of the etched PE membranes in Figure 3. Glucose is much smaller than any of the pores of the newly reported nanoporous PE membrane or the conventional alumina membrane, while the size of albumin falls approximately between their pore dimensions.

Application of such nanoporous membrane is not limited only for separating purpose but also for sensing one. Electrochemical detection of the membrane potential can monitor the amount of the passing-through of the targeted molecules having a size corresponding to a prepared pore diameter. Chemical modification of the pore walls further opens the door of addition of biological functions and intelligences available for the implantable medical devices. Since the targeted molecules pass through nanochannels one by

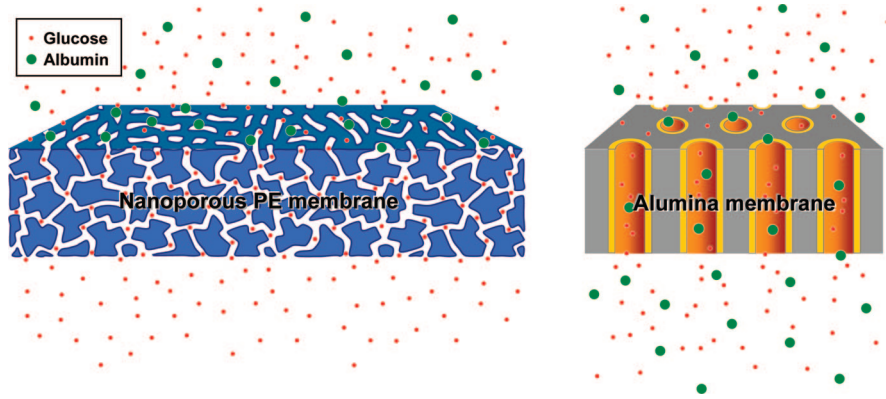

Figure 7. Schematic illustrations of nanoporous membranes for molecular separation. (a) Nanoporous PE membrane prepared in this study. (b) Conventional alumina membrane. The red and green spheres indicate glucose and BSA with radii of 0.76−0.85 and 3.55 nm, respectively.

one, encountering catalysts or enzymes supported on the channel walls can be promised in such molecular-sized "test tubes". The product released by the chemical or biological reactions can be also used as a signal for detection, which plays a similar role to a receptor within the living cell membrane.

CONCLUSION

A series of flexible nanoporous PE membranes was prepared from BCP precursor having a bicontinuous crystalline and amorphous phase-separation system. The obtained nanoporous morphology could be controlled by FNA etching time of these precursory membranes. The mechanical tests for such nanoporous PE membranes indicated their excellent toughness, compared to the conventional alumina nanoporous membrane. Glucose diffusion tests assuming implantable biosensing application suggested that both of these PE and commercial alumina nanoporous membranes can let glucose molecules pass through the thickness direction, but BSA diffusion test results claimed that only the PE membrane can retain the BSA molecules. A combination of size selectivity of molecular diffusion in nanoscale and superior mechanical properties in macroscale for such nanoporous membrane prepared in this study has the potential to lead to advanced biomedical devices having biological functions and intelligences.

METHODS

Membrane Preparation. The material used was polyethylene-*block*-polystyrene (PE-*b*-PS) copolymer purchased from Polymer Source, Inc., in Quebec, Canada. The number-average molecular weights (MWs) were 5.4×10^4 for PS and 6.7×10^4 for PE, with a MW distribution of 1.04. The sample was dissolved into *p*-xylene at its boiling point for 10 min, followed by casting and drying at room temperature in a vacuum. The obtained circular films have a radius of 90 mm and a thickness of 15 or 30 μm. These films were melted at 180 °C and then isothermally crystallized at 90 °C in a vacuum oven for 3 days.

Fuming nitric acid (FNA) etching of the films was performed at room temperature for 5−60 min. An excess amount of FNA (50 mL) was added to 1 g of the above sample film in a glass dish with a cover. Following this etching procedure, the treated film was washed three times with distilled water and ethanol and dried well at room temperature.

For comparison, the asymmetric alumina membrane supplied by Whatman (http://www.whatman.com/PRODAnoporeInorganicMembranes.aspx) was adopted. It has a total thickness of 60 μm, but the active layer is limited to 1 μm thick at the outer surface with 20 nm pores. The other internal portions contain larger but straight pores of 200 nm diameter.

Membrane Characterization. Nanoporous morphologies of the prepared membranes were observed by using a Hitachi field-emission SEM S-4800 operated at 1 kV. Both the membrane surface and cleaved edge were observed. The sample was coated with 5 Å thick Pt−Pd before observation. Pore size was defined as the average width of the longitudinal pores aligned on the membrane surface.

The tensile tests were conducted at room temperature. The specimens were cut into 50 mm long and 5 mm wide strips from the prepared PE nanoporous membrane and commercial alumina membrane. These strips were tensile drawn at a constant cross-head speed, corresponding to an initial strain rate of 1 min^{-1}, in an Orientec Tensilon tensile tester RTC-1325A. Two ends with 10 mm long of the specimen were clumped by the chucks of the tensile tester. Therefore, the actual tensile region was 30 mm long.

Diffusion/Retention Tests. The test cells for the glucose diffusion and albumin retention have two compartments separated by the porous membrane to be tested (Figure 1c). Cell length, *L*, was 5 mm for glucose diffusion tests and 15 mm for albumin retention tests. The tested membrane was sealed between chambers A and B. In order to avoid leakage of the solute of interest, we used an O-ring that was cut out of a PDMS sheet of 1 mm thickness. A membrane was placed onto an O-ring, then two chambers were screwed together. No leakage of solute was confirmed using a nonporous membrane. A solution with a given concentration of the solute of interest is set in the chamber A, and the chamber B is filled with ultrapure water for glucose diffusion test, and with 150 mM aqueous NaCl for albumin retention test, respectively, at the beginning of each experiment. Both chambers were stirred by standard Teflon magnetic stirrers throughout the entire experiment. All the diffusion tests were conducted at room temperature.

Since the surfaces of the prepared nanoporous PE membranes were very hydrophobic, the membranes were first dipped into ethanol to wet the surface and the insides of pores then quickly dipped in water to replace ethanol with water. Each membrane was set in the test cell without drying.

For the glucose diffusion test, a 100 mM D-glucose in ultrapure water solution was put in the chamber A. The glucose concentration of the liquid in the chamber B was measured by refractometry from time to time. The refractometer measurements were made using a Bellingham-Stanley RFM 342 with the 589.3 nm sodium D line. The obtained refractive indices were converted to glucose concentrations using a standard calibration line determined by the plots of the refractive indices for given concentrations of glucose in ultrapure water (see Supporting Information, Figure S1a).

In the albumin retention tests, a 1.0% bovine serum albumin (BSA) solution (also contains 150 mM NaCl) was put in the chamber A, and a 150 mM NaCl solution was put in the chamber B. The liquid in the chamber B was measured with UV spectroscopy using an Ocean Optics USB4000 UV−vis spectrometer with a DT-MINI-2-GC light source. If BSA leaks, a peak at a wavelength of 280 nm should be observed. Therefore, the absorbance at 280 nm was used as an index of the BSA concentration. This BSA retention test was continued for 48 h using BSA with a molecular weight corresponding to 66 kDa and a size of $4 \times 4 \times 14$ nm^3 purchased from Sigma-Aldrich. The standard calibration line was also determined by the plots of the absorbances for given concentrations of BSA (Figure S1b in Supporting Information), the same as for the glucose calibration.

Acknowledgment. This work was partly supported by a Grant-in-Aid for Scientific Research (B) (19350107), The Ministry of Education, Culture, Sports, Science and Technology, Japan. Correspondence and requests for materials regarding nanoporous PE membranes should be addressed to H.U. and regarding glucose and BSA diffusion tests to E.M.

Supporting Information Available: Description of the standard calibration lines for glucose and BSA concentration determinations and SEM images for the 30 μm thick membranes prepared under corresponding etching times. This material is available free of charge *via* the Internet at http://pubs.acs.org.

REFERENCES AND NOTES

1. Gong, D.; Yadavalli, V.; Paulose, M.; Pishko, M.; Grimes, C. A. Controlled Molecular Release Using Nanoporous Alumina Capsules. *Biomed. Microdevices* **2003**, *5*, 75–80.

2. La Flamme, K. E.; Mor, G.; Gong, D.; La Tempa, T.; Fusaro, V. A.; Grimes, C. A.; Desai, T. A. Nanoporous Alumina Capsules for Cellular Macroencapsulation: Transport And Biocompatibility. *Diabetes Technol.* **2005**, *7*, 684–694.
3. Desai, T. A.; Hansford, D. J.; Leoni, L.; Essenpreis, M.; Ferrari, M. Nanoporous Anti-Fouling Silicon Membranes for Biosensor Applications. *Biosens. Bioelectron.* **2000**, *15*, 453–462.
4. Leoni, L.; Boiarski, A.; Desai, T. A. Characterization of Nanoporous Membranes for Immunoisolation: Diffusion Properties and Tissue Effects. *Biomed. Microdevices* **2002**, *4*, 131–139.
5. Yamaguchi, A.; Uejo, F.; Yoda, T.; Uchida, T.; Tanamura, Y.; Yamashita, T.; Teramae, N. Self-Assembly of a Silica-Surfactant Nanocomposite in a Porous Alumina Membrane. *Nat. Mater.* **2004**, *3*, 337–341.
6. Olson, D. A.; Chen, L.; Hillmyer, M. A. Templating Nanoporous Polymers with Ordered Block Copolymers. *Chem. Mater.* **2008**, *20*, 869–890.
7. Jeoung, E. J; Galow, T. H.; Schotter, J.; Bal, M.; Ursache, A.; Tuominen, M. T.; Stafford, C. M.; Russell, T. P.; Rotello, V. M. Fabrication and Characterization of Nanoelectrode Arrays Formed *via* Block Copolymer Self-Assembly. *Langmuir* **2001**, *17*, 6396–6398.
8. Park, C.; Yoon, J.; Thomas, E. L. Enabling Nanotechnology with Self Assembled Block Copolymer Patterns. *Polymer* **2003**, *44*, 6725–6760.
9. Fustin, C.-A; Lohmeijer, B. G. G.; Duwez, A.-S.; Jonas, A. M.; Schubert, U. S.; Gohy, J.-F. Nanoporous Thin Films from Self-Assembled Metallo-Supramolecular Block Copolymers. *Adv. Mater.* **2005**, *17*, 1162–1165.
10. Leiston-Belanger, J. M.; Russel, T. P.; Drockenmuller, E.; Hawker, C. J. A Thermal and Manufacturable Approach to Stabilized Diblock Copolymer Templates. *Macromolecules* **2005**, *38*, 7676–7683.
11. Olayo-Valles, R.; Guo, S.; Lund, M. S.; Leighton, C.; Hillmyer, M. A. Perpendicular Domain Orientation in Thin Films of Polystyrene-Polylactide Diblock Copolymers. *Macromolecules* **2005**, *38*, 10101–10108.
12. Drockenmuller, E.; Li, L. Y. T.; Ryu, D. Y.; Harth, E.; Russell, T. P.; Kim, H.-C.; Hawker, C. J. Covalent Stabilization of Nanostructures: Robust Block Copolymer Templates from Novel Thermoreactive Systems. *J. Polym. Sci., Polym. Chem. Ed.* **2005**, *43*, 1028–1037.
13. Guo, S.; Rzayev, J.; Bailey, T. S.; Zalusky, A. S.; Olayo-Valles, R.; Hillmyer, M. A. Nanopore and Nanobushing Arrays from ABC Triblock Thin Films Containing Two Etchable Blocks. *Chem. Mater.* **2006**, *18*, 1719–1721.
14. Laforgue, A.; Bazuin, C. G.; Prud'homme, R. E. A Study of the Supramolecular Approach in Controlling Diblock Copolymer Nanopatterning and Nanoporosity on Surfaces. *Macromolecules* **2006**, *39*, 6473–6482.
15. Zhang, M.; Yang, L.; Yurt, S.; Misner, M. J.; Chen, J.-T.; Coughlin, E. B.; Venkataraman, D.; Russell, T. P. Highly Ordered Nanoporous Thin Films from Cleavable Polystyrene-*block*-Poly(ethylene oxide). *Adv. Mater.* **2007**, *19*, 1571–1576.
16. Rider, D. A.; Cavicchi, K. A.; Vanderark, L.; Russell, T. P.; Manners, I. Orientationally Controlled Nanoporous Cylindrical Domains in Polystyrene-*b*-Poly(ferrocenylethylmethylsilane) Block Copolymer Films. *Macromolecules* **2007**, *40*, 3790–3796.
17. Nie, Z.; Kumacheva, E. Patterning Surfaces with Functional Polymers. *Nat. Mater.* **2008**, *7*, 277–290.
18. Boudouris, B. W.; Frisbie, C. D.; Hillmyer, M. A. Nanoporous Poly(3-alkylthiophene) Thin Films Generated from Block Copolymer Templates. *Macromolecules* **2008**, *41*, 67–75.
19. Park, S.; Wang, J.-Y.; Kim, B.; Xu, J.; Russell, T. P. A Simple Route to Highly Oriented and Ordered Nanoporous Block Copolymer Templates. *ACS Nano* **2008**, *2*, 766–772.
20. Jeong, U.; Kim, H.-C.; Rodriguez, R. L.; Tsai, I. Y.; Stafford, C. M.; Kim, J. K.; Hawker, C. J.; Russell, T. P. Asymmetric Block Copolymers with Homopolymers: Route to Multiple Length Scale Nanostructures. *Adv. Mater.* **2002**, *14*, 274–276.
21. Yong, S. Y.; Ryu, I.; Kim, H. Y.; Kim, J. K.; Jang, S. K.; Russell, T. P. Nanoporous Membranes with Ultrahigh Selectivity and Flux for the Filtration of Viruses. *Adv. Mater.* **2006**, *18*, 709–712.
22. Zalusky, A. S.; Olayo-Valles, R.; Taylor, C. J.; Hillmyer, M. A. Mesoporous Polystyrene Monoliths. *J. Am. Chem. Soc.* **2001**, *123*, 1519–1520.
23. Zalusky, A. S.; Olayo-Valles, R.; Wolf, J. H.; Hillmyer, M. A. Ordered Nanoporous Polymers from Polystyrene-Polylactide Block Copolymers. *J. Am. Chem. Soc.* **2002**, *124*, 12761–12773.
24. Wolf, J. H.; Hillmyer, M. A. Ordered Nanoporous Poly(cyclohexylethylene). *Langmuir* **2003**, *19*, 6553–6560.
25. Rzayer, J.; Hillmyer, M. A. Nanochannel Array Plastics with Tailored Surface Chemistry. *J. Am. Chem. Soc.* **2005**, *127*, 13373–13379.
26. Rzayer, J.; Hillmyer, M. A. Nanoporous Polystyrene Containing Hydrophilic Pores from an ABC Triblock Copolymer Precursor. *Macromolecules* **2005**, *38*, 3–5.
27. Mao, H.; Hillmyer, M. A. Nanoporous Polystyrene by Chemical Etching of Poly(ethylene oxide) from Ordered Block Copolymers. *Macromolecules* **2005**, *38*, 4038–4039.
28. Mao, H.; Hillmyer, M. A. Macroscopic Samples of Polystyrene with Ordered Three-Dimensional Nanochannels. *Soft Matter* **2006**, *2*, 57–59.
29. Bailey, T. S.; Rzayev, J.; Hillmyer, M. A. Routes to Alkene and Epoxide Functionalized Nanoporous Materials from Poly(styrene-*b*-isoprene-*b*-lactide) Triblock Copolymers. *Macromolecules* **2006**, *39*, 8772–8781.
30. Uehara, H.; Kanamoto, T.; Kawaguchi, A.; Murakami, S. Real-Time X-ray Diffraction Study on Two-Stage Drawing of Ultra-High Molecular Weight Polyethylene Reactor Powder above the Static Melting Temperature. *Macromolecules* **1996**, *29*, 1540–1547.
31. Uehara, H.; Nakae, M.; Kanamoto, T.; Zachariades, A. E.; Porter, R. S. Melt Drawability of Ultra-High Molecular Weight Polyethylene. *Macromolecules* **1999**, *32*, 2761–2769.
32. Nakae, M.; Uehara, H.; Kanamoto, T.; Zachariades, A. E.; Porter, R. S. Structure Development upon Melt Drawing of Ultra-High Molecular Weight Polyethylene: Effect of Prior Thermal History. *Macromolecules* **2000**, *33*, 2632–2641.
33. Uehara, H.; Yamanobe, T.; Komoto, T. Relationship between Solid-State Molecular Motion and Morphology for Ultra-High Molecular Weight Polyethylene Crystallized under Different Conditions. *Macromolecules* **2000**, *33*, 4861–4870.
34. Uehara, H.; Matsuda, H.; Aoike, T.; Yamanobe, T.; Komoto, T. Lamellar Characteristics Controlled by Prior Polymer Concentration for Solution-Crystallized Ultra-High Molecular Weight Polyethylene. *Polymer* **2001**, *42*, 5893–5899.
35. Uehara, H.; Aoike, T.; Yamanobe, T.; Komoto, T. Solid-State 1H-NMR Relaxation Analysis of Ultra-High Molecular Weight Polyethylene Reactor Powder. *Macromolecules* **2002**, *35*, 2640–2647.
36. Uehara, H.; Kakiage, M.; Yamanobe, T.; Komoto, T.; Murakami, T. Phase Development Mechanism during Drawing from Highly Entangled Polyethylene Melts. *Macromol. Rapid Commun.* **2006**, *27*, 966–970.
37. Uehara, H.; Yoshida, R.; Kakiage, M.; Yamanobe, T.; Komoto, T. Continuous Film Processing from Ultra-High Molecular Weight Polyethylene Reactor Powder and Mechanical Property Development by Melt-Drawing. *Ind. Eng. Chem. Res.* **2006**, *45*, 7801–7806.
38. Suwa, J.; Kakiage, M.; Yamanobe, T.; Komoto, T.; Uehara, H. Molecular Weight Segregation on Surfaces of Polyethylene Blend Films as Estimated from Nano-Scratch Tests Using Scanning Probe Microscopy. *Langmuir* **2007**, *23*, 5882–5885.
39. Uehara, H.; Uehara, A.; Kakiage, M.; Takahashi, H.; Murakami, S.; Yamanobe, T.; Komoto, T. Solid-State Characterization of Polyethylene Reactor Powders and Their Structural Changes upon Annealing. *Polymer* **2007**, *48*, 4547–4557.

40. Uehara, H.; Kato, K.; Kakiage, M.; Yamanobe, T.; Komoto, T. Single-Walled Carbon Nanotube Nucleated Solution-Crystallization of Polyethylene. *J. Phys. Chem. C* **2007**, *111*, 18950–18957.
41. Kakiage, M.; Sekiya, M.; Yamanobe, T.; Komoto, T.; Sasaki, S.; Murakami, S.; Uehara, H. Phase Transitions upon Heating for Melt-Drawn Ultra-High Molecular Weight Polyethylenes Having Different Molecular Characteristics. *J. Phys. Chem. B* **2008**, *112*, 5311–5316.
42. Uehara, H.; Takeuchi, K.; Kakiage, M.; Yamanobe, T.; Komoto, T. Nano-Periodic Arrangement of Crystal/Amorphous Phases Induced by Tensile Drawing of Highly Entangled Polyethylene Solid. *Macromolecules* **2007**, *40*, 5820–5826.
43. Uehara, H.; Yoshida, T.; Kakiage, M.; Yamanobe, T.; Komoto, T.; Nomura, K.; Nakajima, K.; Matsuda, M. Nanoporous Polyethylene Film Prepared from Bicontinuous Crystalline/Amorphous Structure of Block Copolymer Precursor. *Macromolecules* **2006**, *39*, 3971–3974.
44. Chan, V. Z.-H.; Hoffman, J.; Lee, V. Y.; Iatrou, H.; Avgeropoulos, A.; Hadjichristidis, N.; Miller, R. D.; Thomas, E. L. Ordered Bicontinuous Nanoporous and Nanorelief Ceramic Films from Self Assembling Polymer Precursors. *Science* **1999**, *286*, 1716–1719.
45. Moscone, D.; Pasini, M.; Mascini, M. Subcutaneous Microdialysis Probe Coupled with Glucose Biosensor for *In Vivo* Continuous Monitoring. *Talanta* **1992**, *39*, 1039–1044.
46. Ballerstadt, R.; Polak, A.; Beuhler, A.; Frye, J. *In Vitro* Long-Term Performance Study of a Near-Infrared Fluorescence Affinity Sensor for Glucose Monitoring. *Biosens. Bioelectron.* **2004**, *19*, 905–914.
47. Lee, S. W.; Shang, H.; Haasch, R. T.; Petrova, V.; Lee, G. U. Transport and Functional Behavior of Poly(ethylene glycol)-Modified Nanoporous Alumina Membranes. *Nanotechnology* **2005**, *16*, 1335–1340.
48. Uehara, H.; Yoshida, T.; Kakiage, M.; Yamanobe, T.; Komoto, T. Structural Arrangement of Crystalline/Amorphous Phases of Polyethylene-*block*-Polystyrene Copolymer as Induced by Orientation Techniques. *J. Polym. Sci., Polym. Phys. Ed.* **2006**, *44*, 1731–1737.
49. Chen, L.; Phillip, W. A.; Cussler, E. L.; Hillmyer, M. A. Robust Nanoporous Membranes Templated by a Doubly Reactive Block Copolymer. *J. Am. Chem. Soc.* **2007**, *129*, 13786–13787.
50. Zhou, N.; Bates, F. S.; Lodge, T. P. Mesoporous Membrane Templated by A Polymeric Bicontinuous Microemulsion. *Nano Lett.* **2006**, *6*, 2354–2357.
51. Hoogervorst, C. J. P.; van Dijk, J. A. P. P.; Smit, J. A. M. Nonstationary Diffusion through Membranes. 1. Transient Diffusion through a Membrane Separating Two Unequal Volumes of Well-Stirred Solutions. *J. Phys. Chem.* **1978**, *82*, 1311–1318.
52. Peinemann, K.-V.; Abetz, V.; Simon, P. F. W. Asymmetric Superstructure Formed in a Block Copolymer *via* Phase Separation. *Nat. Mater.* **2007**, *6*, 992–996.
53. Kosonen, H.; Valkama, S.; Nykänen, A.; Toivanen, M.; ten Brinke, G.; Ruokolainen, J.; Ikkala, O. Functional Porous Structures Based on the Pyrolysis of Cured Templates of Block Copolymer and Phenolic Resin. *Adv. Mater.* **2006**, *18*, 201–205.
54. Savariar, E. N.; Krishnamoorthy, K.; Thayumanavan, S. Molecular Discrimination inside Polymer Nanotubes. *Nat. Nanotechnol.* **2008**, *3*, 112–117.